

Alma Mater Studiorum Università di Bologna
Archivio istituzionale della ricerca

Electrically Controlled "Sponge Effect" of PEDOT:PSS Governs Membrane Potential and Cellular Growth

This is the final peer-reviewed author's accepted manuscript (postprint) of the following publication:

Published Version:

Fabrizio Amorini, Isabella Zironi, Marco Marzocchi, Isacco Gualandi, Maria Calienni, Tobias Cramer, et al. (2017). Electrically Controlled "Sponge Effect" of PEDOT:PSS Governs Membrane Potential and Cellular Growth. ACS APPLIED MATERIALS & INTERFACES, 9(8), 6679-6689 [10.1021/acsami.6b12480].

Availability:

This version is available at: <https://hdl.handle.net/11585/580016> since: 2017-05-10

Published:

DOI: <http://doi.org/10.1021/acsami.6b12480>

Terms of use:

Some rights reserved. The terms and conditions for the reuse of this version of the manuscript are specified in the publishing policy. For all terms of use and more information see the publisher's website.

This item was downloaded from IRIS Università di Bologna (<https://cris.unibo.it/>).
When citing, please refer to the published version.

(Article begins on next page)

This is the final peer-reviewed accepted manuscript of:

Electrically Controlled “Sponge Effect” of PEDOT:PSS Governs Membrane Potential and Cellular Growth

Fabrizio Amorini, Isabella Zironi, Marco Marzocchi, Isacco Gualandi, Maria Calienni, Tobias Cramer, Beatrice Fraboni, and Gastone Castellani

ACS Applied Materials & Interfaces **2017** 9 (8), 6679-6689.

The final published version is available online at:
<http://dx.doi.org/10.1021/acsami.6b12480>

Rights / License:

The terms and conditions for the reuse of this version of the manuscript are specified in the publishing policy. For all terms of use and more information see the publisher's website.

This item was downloaded from IRIS Università di Bologna (<https://cris.unibo.it/>)

When citing, please refer to the published version.

Electrically controlled “sponge effect” of PEDOT:PSS governs membrane potential and cellular growth

Fabrizio Amorini^{1,†}, Isabella Zironi^{,1,†}, Marco Marzocchi¹, Isacco Gualandi¹, Maria Calienni¹, Tobias Cramer¹, Beatrice Fraboni¹ and Gastone Castellani^{1,2}*

¹ Department of Physics and Astronomy, University of Bologna, viale Berti-Pichat 6/2, 40127 Bologna, Italy

² Interdepartmental Centre “L. Galvani” for integrated studies of bioinformatics, biophysics and biocomplexity, Via Zamboni 67, 40126 Bologna, Italy

KEYWORDS: organic conductive polymers; membrane potential; cellular adhesion; cellular proliferation; bioelectronic interfaces; patch clamp

ABSTRACT: PEDOT:PSS is a highly conductive material with good thermal and chemical stability and enhanced biocompatibility that make it suitable for bioengineering applications. The electrical control of the oxidation state of PEDOT:PSS films allows to modulate peculiar physical and chemical properties of the material, such as topography, wettability and conductivity, and thus offers a possible route for controlling cellular behavior. Through the use of: (i) the electrophysiological response of the plasma membrane as a biosensor of the ionic availability; (ii) relative abundance around the cells via X-ray spectroscopy, and (iii) atomic force microscopy to monitor PEDOT:PSS film thickness relative to its oxidation state, we demonstrate that redox processes confer to PEDOT:PSS the property to modify the ionic environment at the film-liquid interface through a “sponge-like” effect on ions. Finally, we show how this property offers the capability to electrically control central cellular properties such as viability, substrate adhesion and growth, paving the way for novel bioelectronics and biotechnological applications.

1. INTRODUCTION

Conjugated polymers (CPs) are a promising material class for bioelectronics and bioengineering applications such as bio-sensing and tissue repairing.^{1,2} Their beneficial properties of biocompatibility³ and biofunctionalization,⁴ along with their electrical, chemical and environmental stability^{5,6} have earned them great attention towards novel applications in electronic medical devices. One of the most interesting feature of CPs is the combined electronic and ionic conductivity and the possibility to modulate their oxidation state in a continuous manner.² Possible consequences of this unique material property are manifold. About two decades ago, was demonstrated that changing the oxidation state of poly-pyrrole (PPy) allows for control of the morphology and growth of adherent mammalian cells.⁷ Since then, most research in this area has been focused on the capability of CPs to electrochemically drive important physiological functions, such as adhesion,⁸⁻¹³ proliferation,^{7,9,12,13} differentiation,¹⁴ cell cross-talking, and secretion, biochemical and electrical signaling.¹⁵⁻¹⁶

Among CPs poly(3,4)-ethylene dioxythiophene (PEDOT) is particularly interesting, due to its high electrical conductivity.^{5,6} PEDOT contains a dioxyalkylene bridging group across the 3- and 4-positions of its heterocyclic ring which greatly improves conductivity and thermal and chemical stability compared to PPy through decreases in band gap and reduction-oxidation potential.¹⁷ Doping of PEDOT occurs via a charge-balanced process in which the positive charge of mobile hole carriers in the polymer backbone is counterbalanced by negatively charged counterions introduced into the polymer. The amount of doping and the chemical nature of the anion determine crucial physical and chemical properties of the conducting polymer/anion composite. One of the preferred anions used in the doping process is Polystyrenesulfonate (PSS) which produces highly

conductive and stable CP composites due to its chemically inert polyanionic structure.¹⁸ PEDOT doped with PSS has shown an improvement in biocompatibility among a wide spectrum of cell types, along with the possibility of obtaining biofunctionalized substrates to improve the biotic / abiotic interface¹⁹. In particular, adhesion and proliferation of human fibroblast²⁰ and epithelial tumor cell lines²¹ are boosted, while the long-term survival of primary neurons^{21,22} and the differentiation process in myoblast are supported,²³ suggesting PEDOT-PSS as an improved electro-ionic interface for a broad range of bio-medical applications.

It is known that the variation in oxidation state of CPs impacts on their peculiar physical and chemical properties, such as topography, wettability^{8,13,24}, mechanical properties^{19,38} and conductivity.²⁵ Oxidation or reduction of conducting polymers requires an uptake or release of ionic species from solution to compensate the variation in electronic charge on the polymer backbone. For example, in conducting polymers that contain large polyanions as dopants such PEDOT-PSS, reduction triggers an uptake of cations to balance the negative charge of the immobile polyanions. The increased amount of cations renders reduced PEDOT-PSS films more hydrophilic²⁵ and can induce swelling in solution.²² Other effects include modification of protein adsorption¹⁹ or field induced conformational changes of the polymers, for example at high applied voltage a reorientation of the hydrophobic groups toward the surface has been observed, decreasing the surface energy and conferring to the polymer film a higher hydrophobicity.^{8,13,24}

The complex interplay of physical and chemical properties of CPs is the critical parameters for cell viability and other behaviors. Nanotopography, for example, can elicit strong effects on cell adhesion, spreading, proliferation and genomic responses in a broad range of cell types.²⁴⁻²⁸ In some cases, it has been suggested that cells can recognize the morphological structures of the adhesion surface through a mechanotransduction mechanism that transduces external mechanical

stimuli into biochemical signals, thus mediating the cell responses.²⁹⁻³¹ Regarding wettability, it was observed that cells adhere, spread, and grow better on surfaces with moderate hydrophilicity due to enhanced adsorption of serum proteins such as fibronectin and vitronectin³² which are crucial for the focal adhesion process. Wettability however, appears as a secondary property compared to the substrate topography.³³ Although these factors suggest that a possible route to control cells functionality with CPs might be based on the physical nano-structure of the surface, our previous studies showed a limited applicability of this approach for PEDOT:PSS based interfaces: CP films with surface roughness ranging from 6 to 33 nm, as obtained by variations in the deposition protocol, did not show a significant trend in cell adhesion and proliferation rate.²⁵ In addition, by testing PEDOT films with different conductive properties, we also excluded the possibility that conductivity could explain variation in cell behaviors. Further, we observed that a relevant enhancement of cell proliferation rate on reduced substrates occurs on different types of PEDOT:PSS used as substrate, and that the modifications in morphology or conducting properties induced by the reduction or oxidation process are separate from the effects on cell behavior parameters. As a consequence of these findings we suggested that the electrochemical state of the conducting polymer must be considered a crucial parameter controlling cellular behavior at the CP/cell interface.²⁵ However, the detailed physicochemical interaction underlying the observed redox-control of cellular behavior remained elusive.

Therefore, in the present work we focused our investigation on modulation of PEDOT:PSS ion exchange relative to its redox state. We used the electrophysiological response of the plasma membrane of two different cell lines (glioblastoma multiforme cells (T98G), and human dermal fibroblasts (hDF)) as biosensors to indirectly measure ionic activities in the medium directly above the exchanging surface. We then correlated these results with cell behavior parameters such as

adhesion ability and proliferation rate. Our findings clearly indicate that the redox state confers to PEDOT:PSS the property to modify the ionic environment around the cells, through a “sponge-like” effect on ions. Furthermore, we verified that cell adhesion and proliferation rates, two biological processes that are tightly correlated to both the ionic equilibrium and the electrophysiology of the cell, are driven by this ionic modulation.

2. EXPERIMENTAL SECTION

2.1. Cell Culture. A Glioblastoma Multiforme cell line (T98G) and primary human dermal fibroblasts (hDF) generously provided by Prof. S. Salvioli (DIMES, University of Bologna) were used in this study. To culture and maintain them in our laboratory we adopted the same protocols used in our previous work.²⁵

2.2. Fabrication of the PEDOT:PSS Substrates. Electropolymerized PEDOT:PSS was synthesized onto glass slides previously coated with spin-coated PEDOT:PSS (commercially available Clevios™ CPP105D) thin films. The deposition solution was prepared by dissolving PSS powder (average molecular weight $\sim 70000 \text{ g mol}^{-1}$) and the pure EDOT monomer in water. The deposition was stopped at 0 V in order to obtain a “*Not biased*” film that exhibits features that are intermediate between the oxidized and reduced substrates. These biased forms were obtained by using PEDOT:PSS films as working electrodes in phosphate buffer solution (PBS), containing (in mM): 150 NaCl; 3 Na₂HPO₄; 1.05 KH₂PO₄ and applying a positive voltage of + 0.8 V (*Oxidized*) or a negative one of - 0.9 V (*Reduced*) using a potentiostat. For further details see our previous work.²⁵

2.3. Adhesion and Proliferation Assay and Analysis. When T98G and hDF cells reached sub-confluence, they were detached by trypsinization (trypsin-EDTA 0.02%) and suspended (1:3) in their respective culture media (supplemented RPMI for T98G and supplemented D-MEM for hDF as described previously) at RT. In order to plate the same number of cells for each substrate, cell counting by the hemocytometer was performed. Adhesion and proliferation properties were tested on a PEDOT:PSS substrate, in its *Not biased*, *Oxidized* and *Reduced* form, and on a culture multiwell plate (CELLSTAR, Greiner bio-one), used as control (*CTRL*). Before cell seeding, PEDOT:PSS substrates, prepared as explained previously, were sterilized under UV light for 30 min, washed out with sterile culture medium and finally fixed to the bottom of a multiwell plate to prevent movement during acquisition. Cells were seeded at a density of $0.010 \times 10^6 \text{ cm}^{-2}$ for T98G and $0.015 \times 10^6 \text{ cm}^{-2}$ for hDF, with 500 μl of respective culture medium. We studied cell adhesion and proliferation with T98G and hDF cells in a CO₂ incubation system integrated within a motorized stage, able to perform time-lapse imaging up to several days. In particular, for adhesion experiments, cells were allowed to adhere for 15 min before the acquisition of images in phase-contrast at 100 \times of magnification for a time interval up to 4 h, every 30 min, with the inverse automated optical microscope Eclipse-Ti (Nikon, Bologna, Italy). The same setup was used also for proliferation, but in this case acquisition was performed every 24 h, up to 96 h (four days). The number of adherent and not-adherent T98G and hDF cells was determined at 2 hours from plating by classifying them according to morphological parameters such as shape (spherical or non-spherical), structural polarization, the presence of lamellar cytoplasm, leading lamella, and clear signs of stress fibers due to the focal adhesion process (Fig. S1). The adhesion rate was defined as the number of adherent cells counted in a focal field of 0.68 mm^2 divided by the total number of

cells. Proliferation analysis was performed by counting all cells present in an image field using ImageJ software and normalizing. The proliferation rates of both cell populations have been estimated by counting the number of adherent cells after 24, 48 and 72 h for the T98G and also 96 h for the hDF (at which time the cell population reached the confluency). The mean number of cells counted in three fixed focal fields sizing 0.68 mm^2 acquired from four wells at each time point was normalized with respect to the number of cells at 24 h from seeding. The results of the independent experiments were reported as mean \pm SEM. Student's t-test was used to estimate the statistical significance; a value of $p = 0.05$ was considered as probability threshold.

2.4. Patch Clamp Recordings and Analysis. Resting membrane potential and voltage-dependent membrane current recordings were measured both using a patch-clamp technique in whole-cell configuration at RT (22-24°C) with an EPC-10 amplifier (HEKA Elektronik, Darmstadt, Germany) interfaced with a compatible computer system equipped with Patch Master software. Before recordings, cells were detached by trypsinization (trypsin-EDTA 0.02%), suspended in 1:3 culture medium and kept out of the incubator in a Falcon tube. Within 6 hours, 30 μl of suspended cells were seeded on a polystyrene 35-mm Nunc Petri dish, used as control (*CTRL*), and on PEDOT:PSS substrates tested in this work. Before seeding, PEDOT:PSS samples were washed out twice with PBS and placed into a Petri dish. After 15 min was controlled the adhesion degree of the cells to the substrates, a wash out with the bath solution was performed and about 2 ml of the same solution was left for recordings. The bath solution (extracellular electrolyte solution), the same for T98G and hDF, contained (in mM): 133 NaCl, 4 KCl, 2 MgCl_2 , 2 CaCl_2 , 10 4-(2-hydroxyethyl)-1-piperazineethanesulfonic acid (HEPES) and 10 glucose (pH 7.4, NaOH). The electrode solution (pH 7.2, KOH) contained, for T98G cells (in mM): 10 NaCl, 120 K-aspartate, 2 MgCl_2 , 4 CaCl_2 , 10 HEPES, 10 ethylene glycol tetraacetic acid (EGTA), 3 Mg-

ATP, 0.2 GTP-Tris, and for hDF cells (in mM): 145 KCl, 1 MgCl₂, 1.8 CaCl₂ and 10 HEPES. After filled the patch pipettes with electrode solution a resistance between 3 and 7 MΩ was obtained.

2.4.1. Voltage-Clamp. Current traces were low-pass filtered at 2.9 kHz and digitized at 20 kHz by using EPC-10 digitizing board. Voltage stimuli (20 mV, 150 ms) from -30 to +110 mV were delivered at intervals of 1 s; to inactivate other voltage-activated K⁺ currents, the holding potential V_h was set to 0 mV. For all recordings specific compensations were used to minimize fast capacitance transients and voltage errors; in this way the software is able to automatically measure cell capacitance. For statistical analysis only the values of the current amplitude traces belonging to a steady-state level were considered averaged to produce a single value for each measurement. To quantify the plasma membrane permeability to potassium ions was used an adjusted bath solution (123 mM NaCl) containing 10 mM of tetraethylammonium chloride (TEA) and was applied by perfusion with a rate of approximately 1-1.5 ml/min. By using the cell membrane capacitance we estimated cellular radius according to the method described by Sakmann and Neher.³⁴ All values were expressed as mean ± S.E.M. Student's t-test was used to compute the probability values (p) in two-group comparison for each voltage step. For statistical significance a threshold of p = 0.05 was considered..

2.4.2. Current-Clamp. Resting membrane potential was acquired through the balanced bridge technology of the EPC-10 amplifier, with the same digitizing rate used for voltage-clamp recordings. Before switching into the current clamp modality the compensation of the capacitance transients in the voltage clamp mode was performed. The membrane current was clamped at 0 pA in order to balance the ionic flows inward and outward the cell. To evaluate the resting membrane potential and in the same time the quality of the seal and the goodness of the recording, we used a

stimulation protocol consisting of current steps (20 pA, 150 ms) from - 120 to + 120 pA delivered at intervals of 1 s. The resting membrane potential value of each cell was obtained by averaging the data from the baseline, i.e. the region of the voltage traces (from 0 to 100 ms) corresponding to the current holding of 0 pA. All values were expressed as mean \pm SEM. Student's t-test was used to compute the probability values (p) in two-group comparison. A p threshold of 0.05 was considered for statistical significance.

2.5. Atomic Force Microscopy. PEDOT:PSS thickness was monitored as a function of time in a phosphate buffer saline solution (PBS) 0.1 M using a Park NX10 atomic force microscopy (AFM) with Park PPP-CONTSCR cantilevers ($k = 0.2$ N/m) in non-contact mode. A potential difference vs Ag/AgCl pseudo-reference electrode was continuously applied to the film using a Pt-wire counter-electrode connected to a Metrohm PGSTAT204. While the AFM recorded continuously a line scan, the potential was switched between an oxidizing (+ 0.8 V) and a reducing (- 0.8 V) value every 100 s. AFM height maps of reduced, neutral and oxidized films were acquired in air.

2.6. Energy-Dispersive X-ray Spectroscopy (EDX). The relative abundance (in atomic %) of K^+ , Na^+ and Cl^- atoms was measured through energy-dispersive X-ray spectroscopy (EDX) using a Cambridge Stereoscan 360 Scanning Electron Microscope (SEM) equipped with an Oxford Instruments X-ray detector. The PEDOT:PSS films investigated with EDX were deposited on a poly(methyl methacrylate) (PMMA) layer, so as to remove the interference coming from K^+ , Na^+ and Cl^- atoms within the usual glass substrate. After PEDOT:PSS deposition, the films were immersed in a solution containing NaCl 0.1 M and KCl 0.1 M and a potential difference of + 0.8 V (*Oxidized*) or - 0.9 V (*Reduced*) vs SCE reference electrode was applied for 1 h. As a control,

we did the same with PEDOT:PSS films not biased. The data obtained were normalized to the relative abundance of K atoms in the not biased PEDOT:PSS film.

3. RESULTS

To better understand the physiological adaptation of cultured cells to biased and not biased PEDOT:PSS substrates we focused our attention on different biological responses, i.e. adhesion capability, proliferation boost, voltage-dependent ion current and resting membrane potential of glioblastoma multiforme cells (T98G). The stability of this cell line, the high proliferation rates, the lack of contact inhibition and replicative senescence, are peculiar features that, along with a domain of potassium (K^+) channels expressed on the plasma membrane, made this an ideal model for our purposes. However, we tested also the primary human dermal fibroblasts (hDF), as a model of healthy cell. Therefore, in the final paragraph of this section, we proposed a comparison between the results of the resting membrane potential values obtained for both the T98G and hDF cell types (for further information regarding hDF results see *Supporting Information*).

Experiments were performed seeding the cells on a polystyrene substrate of standard cell culture plates, used as control (*CTRL*) and on all the three types of PEDOT:PSS substrates here investigated: *Not biased*, *Oxidized* and *Reduced*, fabricated by electrodeposition through 8 cycles of cyclic voltammetry as described in “*Experimental section*”

3.1. Adhesion Rate of the T98G cells is PEDOT:PSS Redox State Dependent. We observed that the adhesion properties of the T98G cells are enhanced when the PEDOT:PSS substrate has been biased: the adhesion rate of cells plated on the *Oxidized* (52.2 ± 1.3 %, $n=12$) or *Reduced* (63.5 ± 1.1 %, $n = 13$) significantly increases compared to the *Not biased* (30.6 ± 2.1 %, $n = 14$) with a $p \ll 0.001$ for both comparisons (Fig. 1A). It is relevant that substrates in the reduced form

exert a stronger effect than the oxidized ones ($p < 0.001$), suggesting that these act in different ways on the adhesion process. Furthermore, we observed a decreased adhesion capability on the *Not biased* that is about 50% lower compared to the *CTRL* ($58.3 \pm 0.8 \%$, $n = 21$). These results suggest that the not biased substrate itself might affect the cell adhesion process.

3.2. Proliferation Rate of the T98G cells is PEDOT:PSS Redox State Dependent. The results shown in Fig. 1B reveal that the T98G proliferation function is positively affected by the oxidized (2.7 ± 0.1 , $n = 5$) and the reduced (3.9 ± 0.4 , $n = 5$) forms of the PEDOT:PSS substrate compared to the not biased one (2.0 ± 0.2 , $n = 6$), matching the adhesion results. Indeed, at 72 h after seeding (the confluence time for our samples), the proliferation rate of cells growing on the biased PEDOT:PSS was significantly higher compared than that obtained for the *Not biased* samples ($p < 0.05$ and $p < 0.005$, respectively for *Oxidized* and *Reduced*). This effect seems to be more relevant on the *Reduced*, being already significantly different at the beginning of the growth curve (after 48 h from seeding) and stronger at the confluency when compared to the *Oxidized* ($p < 0.05$). Furthermore, in order to display the effect of the pristine form of PEDOT:PSS we also compared the data obtained from T98G growing on the *CTRL* and on the not biased substrates. The cell population showed a significantly higher proliferation rate on the *CTRL* only at 72 h. Despite these results, the proliferation rate increment at the confluence time point (72 h) on the *Reduced* sample is by three times as much the value at time 0 (24 h), suggesting a strong efficiency of this specific redox state on cellular replication.

3.3. PEDOT:PSS Redox State Affects the Electrical Properties of the T98G cells.

3.3.1. Whole-Cell Current Recordings. The results described thus far show that cell adhesion and proliferation processes are strongly correlated with the redox state of PEDOT:PSS. We know already that these processes, beside other pathways, are dependent on K^+ channels activity.³⁵⁻³⁷ In

parallel, redox processes in PEDOT:PSS substrates are accompanied by ion-migration across the film-liquid interface.² We therefore directed our attention to the electrical properties mediated by intra- and extra-cellular ionic concentrations., and transmembrane whole-cell currents were recorded in voltage-clamp mode from T98G cells plated on *CTRL* and on *Not biased*, *Oxidized* and *Reduced*. In order to single out the K^+ current from the overall current recorded we did a set of experiments using the non-selective K^+ channel's inhibitor tetraethylammonium chloride (TEA) at the saturating concentration of 10 mM. In the *Supporting Information* section we show that T98G cells displayed an outward current whose amplitude, at 110 mV of voltage potential, is about 1257 ± 74 pA ($n = 16$) that is almost completely blocked by perfusion with TEA (128 ± 20 pA, $n = 9$) (Fig. S2). No other currents were revealed by our analysis, indicating that the current recorded is predominantly due to ion fluxes through outward K^+ channels. Representative examples of the current traces recorded on *CTRL* and on *Not biased*, *Oxidized* and *Reduced* are reported in Fig. 1C, which compares mean current amplitudes relative to each voltage step (I-V curve) recorded from T98G cells plated on *CTRL* with those plated on each different form of PEDOT:PSS substrates. The statistical analysis shows that the amplitude of K^+ current recorded is not affected by the *Not biased*. Interestingly, both the *Oxidized* (1549 ± 120 pA at 110 mV, $n = 14$) and the *Reduced* (843 ± 70 pA at 110 mV, $n = 15$) appear to act as consistent effectors, significantly changing the amplitude of the current compared to the *Not biased* (respectively $p < 0.01$ and $p < 0.001$ at 110 mV of voltage stimulation) (Fig. 1D). Data from voltage clamp recordings from cells plated on *CTRL* and PEDOT:PSS substrates are summarized in Table S1 (*Supporting Information*), which in addition to current amplitude evoked by + 110 mV of voltage step gives values (\pm SEM) of the membrane capacitances and relative cellular radius, was estimated by the spherical capacitor-capacitance relationship.³⁴

3.3.2. *Resting Membrane Potential Recordings.* The electrical properties of cells due to ion channel activity and the intensity of ion fluxes strongly correlate to the resting membrane potential (V_{rest}) value. Taking into account the previous results, it becomes central to determine whether and how V_{rest} is affected in the presence of the biased forms of PEDOT:PSS. Therefore, the resting potentials of T98G cellular membranes were recorded from cells plated on *CTRL*, *Not biased*, *Oxidized* and *Reduced* in current-clamp mode (whole-cell current clamped at 0 pA). Averaged values of V_{rest} and statistical significances are displayed in Fig. 1E and contained in Table S1 (*Supporting Information*). These results show that V_{rest} is affected by the not biased substrate by inducing a depolarization which increases in the biased samples from the *Oxidized* to the *Reduced*. In more detail, we found significant differences ($p < 0.01$) in the V_{rest} values obtained from T98G when plated on the *CTRL* substrates compared to the *Not biased*. Assessing V_{rest} for *Oxidized* and *Reduced*, we found a significant difference compared to the *Not biased* only for *Reduced* ($p < 0.001$). Thus, the most significant finding is that *Reduced* induces the largest depolarization of V_{rest} .

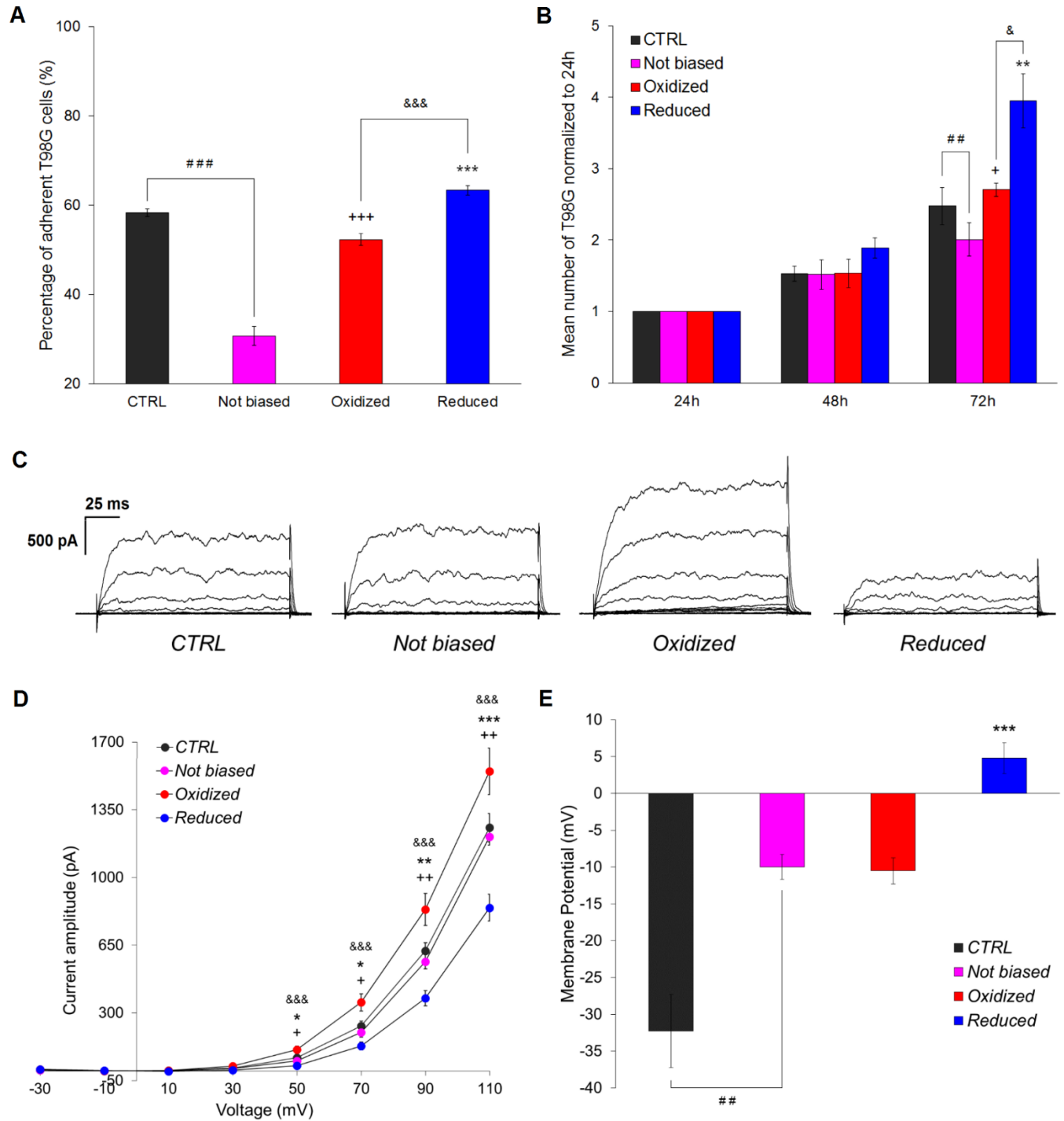


Figure 1. Effects of PEDOT:PSS at different redox forms on T98G adhesion, proliferation and electrophysiology. (A) Adhesion rate: percentage \pm SEM of adherent T98G after 2 h from seeding on polystyrene Petri dish (CTRL, $n = 21$) and on *Not biased* ($n = 14$), *Oxidized* ($n = 12$) and *Reduced*

(n = 13). **(B)** Proliferation rate: mean number \pm SEM of T98G cells counted at 24, 48 and 72 h (confluence) and normalized to data obtained at 24 h from seeding. Cells were plated on *CTRL* (n = 5) and on *Not biased* (n = 6), *Oxidized* (n = 6) and *Reduced* (n = 6). **(C)** Comparison of representative examples of whole-cell current traces recorded in T98G seeded on *CTRL* and on PEDOT:PSS substrates. **(D)** Average \pm SEM of current-voltage relationships (I–V) recorded in T98G plated on *CTRL* (n = 16), *Not biased* (n = 14), *Oxidized* (n = 14) and *Reduced* (n = 15). **(E)** Average \pm SEM of the resting membrane potential recorded in T98G seeded on *CTRL* (n = 11), *Not biased* (n = 7), *Oxidized* (n = 13) and *Reduced* (n = 10). *CTRL* vs *Not biased*: ##p<0.01, ###p<0.001; *Not biased* vs *Oxidized*: +p<0.05, ++p<0.01, +++p<0.001; *Not biased* vs *Reduced*: *p<0.05, **p<0.01, ***p<0.001; *Reduced* vs *Oxidized*: &p<0.05, &&&p<0.001. All p values were calculated by Student's t-test.

3.4. Testing a Different Type of Cell. In order to validate our results in healthy cells, the same experiments were performed in hDF, which are characterized by a very similar set of ionic channels expressed on the plasma membrane but are more comparable to physiological conditions. We observed that, unlike the T98G cells, no significant differences (or very mild) in adhesion and proliferation rates were observed between the biased forms of PEDOT:PSS and the not biased ones. These results strongly correlate with the data obtained by the electrophysiological analyses, indeed both V_{rest} and voltage-dependent ionic currents are not affected by the *Oxidized* and the *Reduced* (Fig. S3). Specifically, in Fig. 2, we compared the V_{rest} of T98G and hDF indicating that the resting condition of the two cell types on *CTRL* are significantly different ($p < 0.005$), showing the T98G cells a more hyperpolarized plasma membrane. This difference in the starting point of the V_{rest} could be the key to understanding why all the redox forms of PEDOT:PSS are not able to

change the V_{rest} itself and to modulate the behaviour of hDF in the same way to what was observed for T98G.

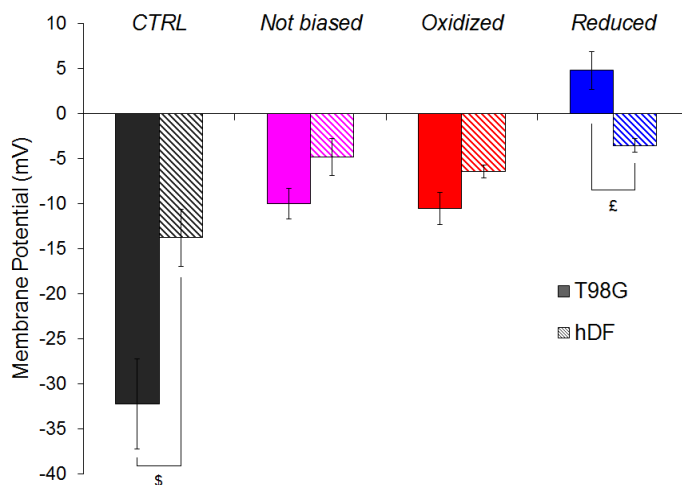


Figure 2. Comparison between resting membrane potential recorded in T98G and hDF cells. Average \pm SEM of the resting membrane potential whole-cell recorded in T98G (solid colours) and hDF (diagonally striped colours) after seeding on *CTRL* (T98G $n = 11$, hDF $n = 12$) and on PEDOT:PSS *Not biased* (T98G $n = 7$, hDF $n = 9$), *Oxidized* (T98G $n = 13$, hDF $n = 7$) and *Reduced* (T98G $n = 10$, hDF $n = 9$). *CTRL* (T98G) vs *CTRL* (hDF): $\$p < 0.005$; *Reduced* (T98G) vs *Reduced* (hDF) $\text{£}p < 0.005$. All p values were calculated by Student's t -test.

3.5. Swelling Properties of PEDOT:PSS. As a first experiment, we characterized the swelling of the PEDOT:PSS film as a function of its oxidation state. To this end, we performed AFM measurements in buffer solution (PBS) under electrochemical control using reference and counter electrode. The variation of PEDOT:PSS film thickness, Δz , as measured while the polymer film is cycled between a reduced (negative potential) and oxidized (positive potential) state is displayed

in Fig. 3. Variation of the potential leads to a characteristic fluctuation in the height of the film with a peak-to-peak amplitude of about 50 nm (10% of film thickness). The time scale of this swelling process was found to be on the order of tens of seconds. In the reduced state (negative potential) the extension of the film was maximized, while oxidation led to shrinking. We remark that in this calibration experiment the redox potential of PEDOT:PSS was actively controlled. During biological experiments, changes in the PEDOT:PSS redox state occurred on a longer time scale, following an exponential decay towards an intermediate state (Fig. S4). In order to investigate the possible impact of redox-processes on the surface topography of PEDOT:PSS films, we acquired AFM height maps for the reduced, neutral and oxidized films (Fig.3, top). All three films exhibit the characteristic cauliflower morphology of electropolymerized PEDOT:PSS with nanometric globular extensions at the surface. In the reduced state, the globular extensions at the surface are slightly enlarged which is attributed to the swelling. Accordingly, also the roughness in the reduced state was slightly enlarged. On 5 μm maps we found rms-roughness values of 15.5 \pm 2.2 nm, 9.8 \pm 2.2 nm and 11.0 \pm 2.8 nm, for reduced, neutral and oxidized films, respectively. We note that these differences in surface topography are small and cannot be expected to account for the observed changes in cell behavior; larger variations on PEDOT:PSS surface topography (for example control of roughness ranging from 6 nm to 33nm) can be obtained by varying electropolymerization conditions, which were reported to not exhibit significant impact on cells.²⁵

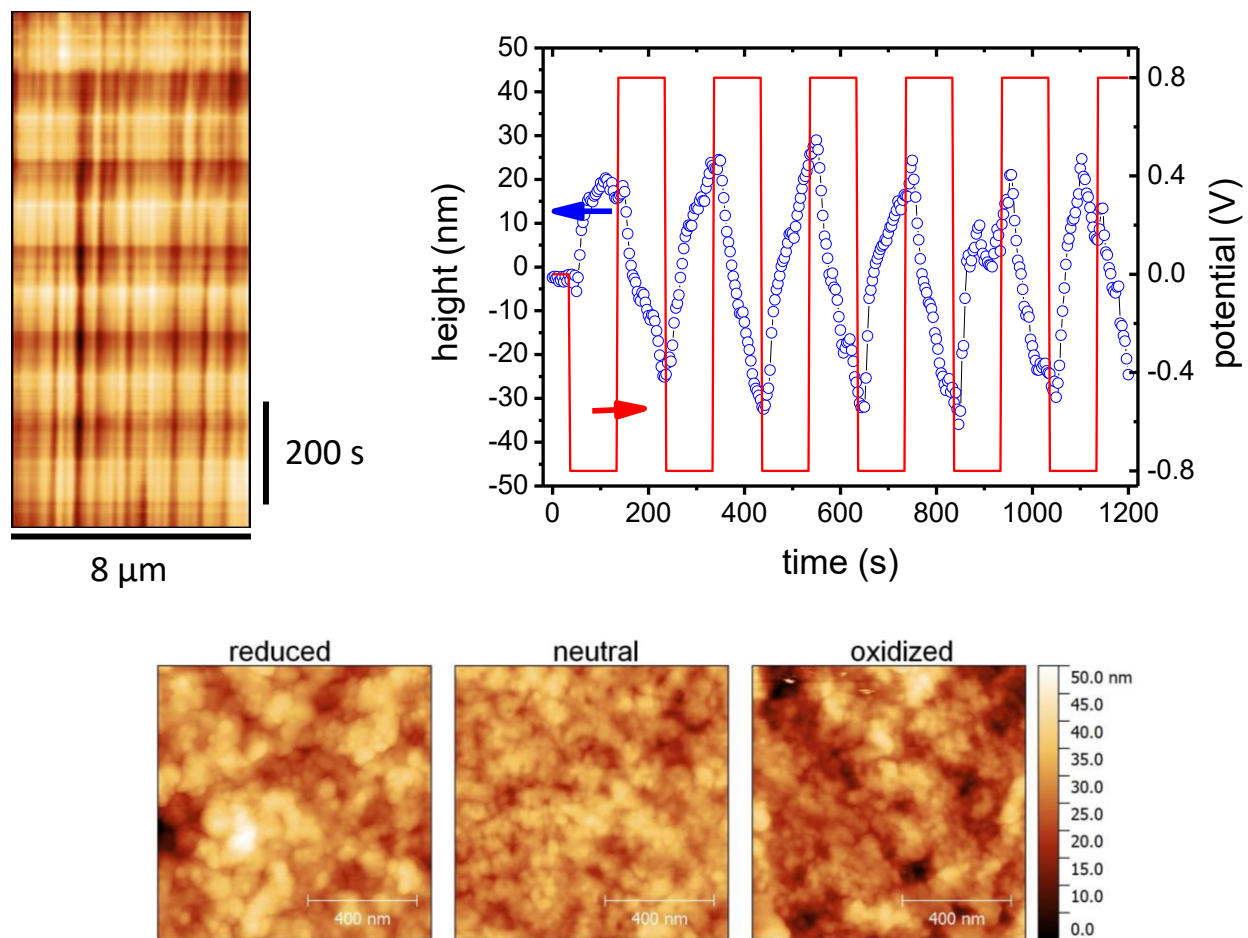


Figure 3. Investigation of impact of potential on PEDOT:PSS film morphology and film thickness by AFM (non-contact mode). *Top left:* height line scan (x-direction) continuously measured for 1200 s (y-direction) while the potential applied to PEDOT:PSS film immersed in PBS was varied between + 0.8 V and - 0.8 V. *Top right:* height of a single point in the linescan (blue, left scale) and applied potential (red, right scale) as a function of time. Negative potential yielded an increase in height due to redox mediated swelling; *bottom:* height maps of reduced, neutral and oxidized PEDOT:PSS film.

3.6. Testing Ion Concentrations and Migration Dynamics in PEDOT:PSS. We used EDX to quantify the amount of ion uptake during oxidation or reduction of PEDOT:PSS substrates in

electrolyte solution. Fig. 4 reports the atomic percentages of Na^+ , K^+ and Cl^- ions as well as the sum of K^+ and Na^+ (cations) for the three investigated cases. Both biased samples, *Oxidized* (2.4 ± 0.3 , $n = 3$) and *Reduced* (10 ± 1 , $n = 3$), showed a significantly increased amount of cations compared to the *Not biased* (1.6 ± 0.3 , $n = 3$) with a $p < 0.05$ for both comparisons (Table 1). It was also observed that cation adsorption was enhanced in the reduced form with respect to the oxidized one ($p < 0.001$). The K^+ level was not statistically different between *Oxidized* (0.7 ± 0.2 , $n = 3$) and *Not biased* (1.0 ± 0.2 , $n = 3$), while *Not biased* and *Reduced* were significantly different with a $p < 0.005$. Conversely, the Na^+ level for *Not biased* (0.6 ± 0.2 , $n = 3$), *Oxidized* (1.7 ± 0.3 , $n = 3$) and *Reduced* (6.0 ± 0.7 , $n = 3$) were significantly different with $p < 0.01$ for all the comparisons. Moreover during the oxidation process, Cl^- anions penetrated into PEDOT:PSS as suggested by a normalized Cl^- content of 0.4 ± 0.1 . On the other hand, *Reduced* and *Not biased* exhibited a Cl^- signal that was lower than the limit of detection of the EDX analyzer. All results are summarized in Table 1.

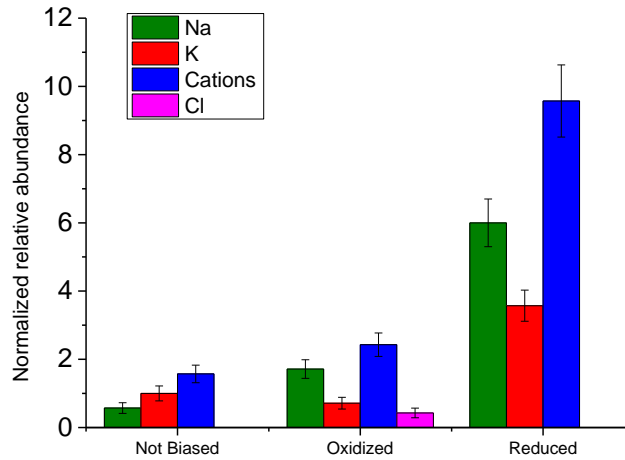


Figure 4. Relative abundance of Na, K and Cl ions in not biased, oxidized and reduced PEDOT:PSS films. The data were normalized to the K abundance recorded for not biased

PEDOT:PSS film. The overall presence of positive ions absorbed by PEDOT:PSS, given by the sum of Na and K concentrations, is represented by the label “Cations”.

Table 1. Relative abundance (average \pm standard deviation) of Na, K and Cl in not biased, oxidized and reduced PEDOT:PSS films. The overall presence of positive ions absorbed by PEDOT:PSS, given by the sum of Na and K concentrations, is represented by the label “Cations”.

	Na	K	Cations	Cl
Not biased	0.6 ± 0.2	1.0 ± 0.2	1.6 ± 0.3	0.0
Oxidized	1.7 ± 0.3	0.7 ± 0.2	2.4 ± 0.3	0.4 ± 0.1
Reduced	6.0 ± 0.7	3.6 ± 0.5	10 ± 1	0.0

4. DISCUSSION

First, we consider the changes in the PEDOT:PSS film caused by oxidation or reduction. Our AFM and EDX experiments showed that the PEDOT:PSS redox state impacts on the volume of the film and on the concentration of ions. The findings have been explained by electrochemical processes and electroswelling³⁸ occurring during the application of a potential to a conducting polymer film in contact with an electrolyte (Fig. 5). During reduction (negative potential), electrons enter into the film and reduce the amount of positive charge on the PEDOT chains. To maintain electroneutrality, cations (i.e. Na^+ and K^+) migrate from the solution into the film and counter-balance the negative charge on immobile PSS polyanions. The large influx of cations leads to swelling of the PEDOT:PSS film. Instead oxidation removes electrons from PEDOT and thus augments the amount of positive charge. The resulting higher charge density then leads to formation of polaronic structures which strongly interact electrostatically with the negatively

charged PSS, thus reducing film volume. As a second competitive process during oxidation, irreversible over-oxidation sets in (Fig. S5), which leads to the formation of neutral, sulfoxide containing units in PEDOT.^{39,40} As a consequence of over-oxidation, some cations migrate into the film to neutralize the PSS negative charge. The three investigated PEDOT:PSS redox states (*Not biased*, *Oxidized* and *Reduced*) thus differ significantly in ion-concentration and volume and we consider the PEDOT:PSS film to act as an electrically controlled nano-sponge for cations. Importantly, during cell-culture experiments, the PEDOT:PSS film is no longer biased and its redox-state starts to shift towards the neutral state, following the de-biasing curve shown in Fig. S4. Charged films consequently release incorporated ions at a slow time-scale of hours when measurements are done at physiological ionic strength. The redox state defines which and how many ions are absorbed, and afterwards released (Fig. 5).

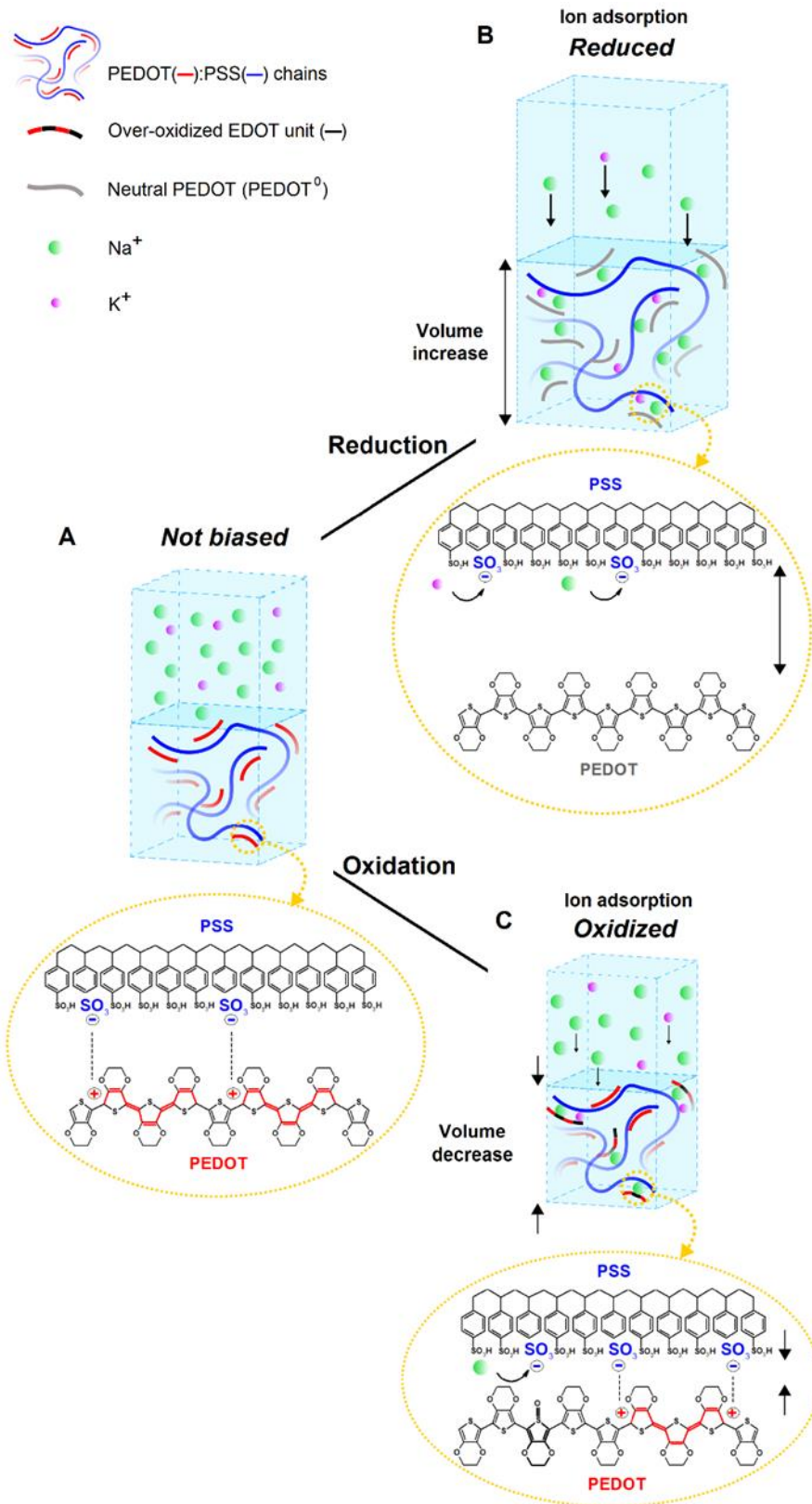


Figure 5. Schematic representation of the nano-sponge mechanism. (A) Section of the not biased PEDOT(red):PSS(blue) substrate immersed in PBS (light blue) and an insert of its chemical structure. (B) The application of a negative potential (- 0.9 V, 1 h lasting) reduces PEDOT that loses its positive charges becoming neutral (grey). Thus the binding between the SO_3^- groups of PSS and PEDOT is partially removed, and cations coming from the electrolyte solution (PBS), are electrostatically attracted to the negative charges of the SO_3^- groups and thus migrate into the polymer film (big arrows). The increased ionic content leads to swelling and an increase in film thickness. (C) The application of a positive potential (+ 0.8 V, 1 h lasting) oxidizes PEDOT. Two different competitive processes take place: i) the positive charge on PEDOT increases; ii) some EDOT units degrade irreversibly (over-oxidation, Fig. S5) binding other chemical species leaving the negative charges of PSS unpaired. Thus, due to the high hydrophilicity of PSS and the porous structure of PEDOT:PSS, some cations are still withheld into the polymer matrix (small arrows), but the adsorption capability is significantly lower compared to the reduced one. The electrostatic binding between PEDOT and PSS becomes tighter, and the film thickness decreases (Fig. 3).

The continuous release of ions from the surface impacts on the electrophysiology of adherent cells. The resting membrane potential (V_{rest}) of cells is in general set by the balance between the intra- and extra-cellular ion concentration regulated by the type and properties of passive (leakage) and voltage-gated membrane channels. In particular, in T98G cells plated on the control substrate (polystyrene Petri dish) we observed a V_{rest} of about -40 mV. Considering that the overall outward current is mainly due to K^+ ion flow (Fig. S2) we would have expected to observe a V_{rest} similar to the equilibrium potential for the K^+ ion (about -90 mV). Furthermore, we observed that no inward current can be induced by voltage potential stimuli lower than -30 mV (data not shown) and that, as reported by Olsen and Sontheimer,⁴¹ this is primarily due to an absence of inwardly

rectifying K^+ channels (K_{ir}). As a result, we can expect an accumulation of K^+ ions in the extracellular solution and thus a depolarization of the plasma membrane.⁴¹ Therefore, the very simple setting of the T98G V_{rest} and strict dependency on the K^+ electrochemical driving forces, make this cell line a very good model to investigate the redox state of PEDOT:PSS, utilizing its electrical properties as a biosensor probe. In this light, it is clear that small changes in the external K^+ concentration, especially those localized at the film-liquid interface, might be capable to interfere with the Nernst equilibrium, thus modifying the diffusive gradient and, consequently, changing V_{rest} . In particular, we know that membrane depolarization occurs for increasing extracellular K^+ concentration and associated decreasing driving force for K^+ efflux.⁴² Similarly, when the extracellular K^+ concentration increases due to the release of K^+ previously adsorbed by the PEDOT:PSS substrates, V_{rest} depolarization occurs (Fig. 1E and Fig. 6). Indeed, in accordance with the “nano-sponge” effect, the V_{rest} recorded from cells plated on PEDOT:PSS substrates goes through a depolarizing trend from the control to the not biased form (with a V_{rest} recorded very similar to the oxidized one) and then to the reduced form following the schematic mechanism described in Fig. 5 and Fig. 6.

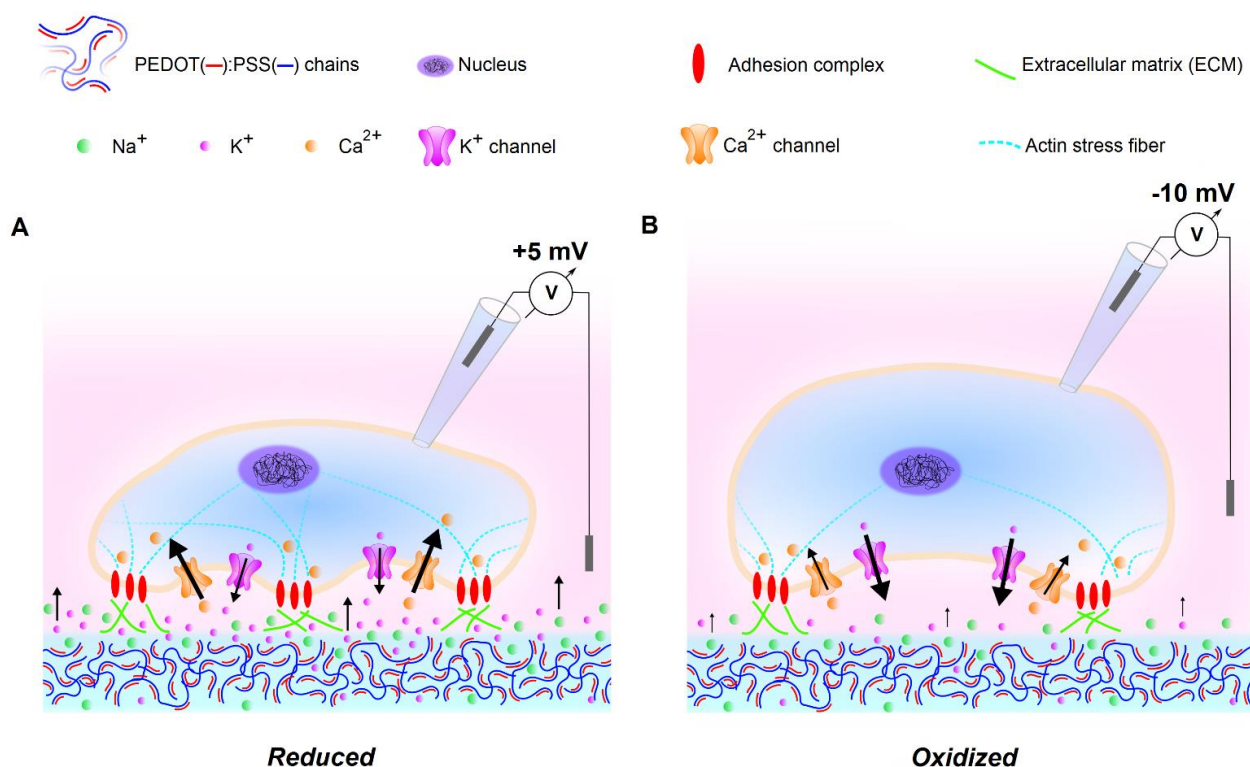


Figure 6. Schematic representation of the nano-sponge effects on electrochemical cellular equilibrium. Immediately after the polarization process, cells are plated on PEDOT:PSS substrates. Following a de-biasing/time curve the polymeric matrix relaxes, allowing ions to diffuse into the cell culture medium (light pink). Cations are thus released and the ionic concentration changes at the film-liquid interface, where cells adhere, as a function of the redox state: **(A)** PEDOT:PSS reduced substrate releases cations, increasing their extracellular concentration. Consequently, the diffusive strength across the cell membrane decreases, lowering the outward K^+ current (small arrows) and depolarizing the plasma membrane (+ 5 mV) which enhances the inward flow of Ca^{2+} (big arrows). This new electrochemical equilibrium boosts the adhesion process and encourages the progress of the cell cycle; **(B)** PEDOT:PSS oxidized substrate releases a lower number of cations leading to a similar but milder effect than that observed for the reduced substrate, due to a higher K^+ current (big arrows), more polarized membrane potential (- 10 mV) and lower Ca^{2+}

current (small arrows), resulting in slower adhesion and proliferation rates (see discussion for details).

We also observed that different redox states of PEDOT:PSS exhibit different effects on outward K^+ currents (Fig. 1D). The membrane stimulation of T98G cells by voltage steps (maximum = 110 mV), showed that the outward current reached the same values when cells were plated on the control and not biased substrate, while an increase was observed on the oxidized condition and a decrease on the reduced condition. The greatest contribution to the whole-cell ionic currents in T98G cells is due to high conductance Ca_2^{+} -activated voltage-gated K^+ channels (BK), which are precisely modulated by the intracellular Ca_2^{+} concentration.⁴³ The opening of voltage-gated-calcium-channels (VGCCs) at membrane depolarization greater than -40 mV allows an inward Ca_2^{+} flow⁴⁴ resulting in increased BK channel activity. This upregulation, the increased concentration of cations in the medium around the cells due to release from the PEDOT:PSS substrates, significantly affects the diffusive gradient of K^+ across the cell membrane. This is true especially for the reduced condition, where the release of a higher amount of cations induced a reduction in K^+ outward flow. In accord with this, only the oxidized substrate showed a slight increase in the current amplitude, and this is the condition which appears to release the least amount of K^+ . These effects are likely to be balanced in the not biased form. Therefore, we can conclude that the resting membrane potential and outward current amplitude data obtained from cells plated on the different forms of PEDOT:PSS are in good agreement with the ion adsorption and release capabilities of PEDOT:PSS shown in the EDX results, confirming that the “nano-sponge” effect can be applied to modulate the cell electrical functions.

The redox forms of PEDOT:PSS are also responsible for strong changes in cellular adhesion properties and cell proliferation. We observed that these two parameters obtained from T98G

cells plated on the oxidized and the reduced substrates increased compared to the not biased substrates, matching the same trend of the V_{rest} (Fig. 1). It has been recently found that membrane depolarization affects endothelial cell stiffness by influencing the polymerization state of cortically located actin filaments.⁴² Therefore, for example in depolarized T98G cells such as those plated on the reduced PEDOT:PSS substrate, it might be reasonable to expect a better and faster adhesion compared to stiffer cells plated on relatively less depolarizing substrates such as the not biased or the oxidized ones (Fig. 6). Furthermore, it is known that the intracellular Ca^{2+} availability plays a key role in the adhesion process through regulation of many of the molecular pathways essential for cell movement, such as the dynamics of the actin cytoskeleton and the formation and disassembly of cell–substratum complexes.⁴⁵ Thus, an increase of the cytosolic Ca^{2+} availability at the first steps of the focal adhesion process, consistent with T98G cells that show a plasma membrane polarized over -40 mV, might result in a better-triggered machine improving adhesion capability.

Studies performed on a human malignant carcinoma cell line demonstrated that during the G1/S transition, multiple families of voltage dependent K^+ channels become active, including BK.⁴⁶ Moreover, it was recently observed that K^+ channels expression or activity changes across the stages of the cell cycle, resulting in a modulation of the cell membrane potential that undergoes considerable fluctuations. For example, the pre-mitotic phase of replicating cells exhibits reduced K^+ channels functionality and a significantly depolarized membrane potential.³⁷ This is in agreement with previous findings reporting that sustained depolarization is able to induce DNA synthesis and mitosis in cells.⁴⁷ Furthermore, for many years Ca^{2+} has been recognized as a strategic mediator of intracellular signals implicated in the control of mitogenic pathways,⁴⁸ and thus its intracellular increase in depolarized cells may trigger mechanisms required for cell proliferation

and accelerate the replicative boost. Accordingly, the increased proliferation rate that we observed on the reduced PEDOT:PSS form can be explained by the capability of the “nano-sponge” effect of induce the V_{rest} depolarization, which encourages the overcoming of the checkpoint between the phase G2 and M of the cell cycle and supports the replicative process. All the above results indicate that K^+ ion driving forces play a crucial role in modulating the replication of tumor cells. The depolarization of the membrane potential was also observed in the oxidized and not biased substrates, but less evident as expected.

We also tested the effects of the redox state of PEDOT:PSS on a different type of cell (hDF). In this case we observed that the material ion exchange capability is unable to sufficiently modulate the plasma membrane responses, as well as the adhesion and proliferation rates, and that these remain very similar for all the PEDOT:PSS forms tested (Fig. S3). We suggest that this behavior might be due to the different electrophysiological resting state of hDF; indeed, these cells show a value of V_{rest} that is much more depolarized and a whole-cell outward current amplitude much smaller (Fig. S3), practically halved, compared with the results obtained for T98G plated on control Petri dish. These observations point to a less reactive electrophysiological setup for hDF cells, and to lower driving forces for the cations outward fluxes, thus leading, in the case of extracellular ionic concentration increases, to under-threshold effects.

5. CONCLUSIONS

The tests we carried out clearly indicate that, while the “sponge effect” offers the opportunity to actively change the availability of ionic species around the cell, the key actors in setting the intensity and the dynamic of the cell response, even in terms of adhesion and proliferation boost, are the cell/substrate intrinsic bioelectrical properties. Using a tumor cell line, we clearly have

shown that the redox state of PEDOT:PSS can elicit strong effects on the behavior of cells through a modulation of the electrochemical equilibrium. In our model we focused on K^+ but other types of cations and anions could be specifically included through doping into the PEDOT:PSS film, potentially allowing for control of a variety of cellular processes linked to the specific bioelectrical features of the doped PEDOT:PSS substrate. This new result paves the way for future applications of bioelectronics and biotechnology directed towards controlling the behavior of a wide range of cells and tissues.

ASSOCIATED CONTENT

Supporting Information

Representative example of cell morphological changes during the adhesion process to PEDOT:PSS substrate; current-voltage relationships (I–V) obtained in T98G before and after tetraethylammonium (TEA) application; adhesion, proliferation and electrophysiological results obtained with human dermal fibroblast plated on the different redox forms of PEDOT:PSS and comparison with those obtained with T98G cells; PEDOT:PSS de-biasing curves recorded in D-MEM and water after the polarization process, characterization of the PEDOT:PSS substrates by cyclic voltammetry in order to prove that over-oxidation occurs also at + 0.8 V and table of mean values of whole-cell current amplitude, capacitance, radius and resting membrane potential obtained from recordings of T98G and hDF cells seeded on the substrates studied in this work.

This material is available free of charge via the Internet at <http://pubs.acs.org>.

AUTHOR INFORMATION

Corresponding Author

* E-mail: isabella.zironi@unibo.it

Author Contributions

F. A.[†] performed the patch clamp experiments, analyzed and interpreted the data, wrote the paper; I. Z.[†] conceived and designed the experiments, performed the growth experiments, interpreted the data and wrote the paper; M. M. and I. G. fabricated and characterized the PEDOT:PSS thin films; M. C. analyzed the electrochemical data; T. C. performed the AFM experiments; B. F. conceived and coordinated the experiments related to PEDOT:PSS structure and properties; G. C. conceived the experiments, analyzed the data and wrote the paper. All authors discussed the experimental data and contributed to writing the manuscript.

[†] These authors contributed equally to this work.

Notes

The authors declare no competing financial interest.

ACKNOWLEDGMENTS

The authors thank David Muehsam for his help in revising the manuscript and acknowledge support by the Bologna University project “Beyond Animal Testing: a Multi-Active Nanostructured device mimicking in vivo environments” FARB-UNIBO (2014-2016). BF, MC, IG and MM acknowledge funding from the Italian Ministry of Research under the PRIN funding scheme.

REFERENCES

- (1) Nikolou, M.; Malliaras, G. G. Applications of Poly(3,4-ethylenedioxythiophene) Doped with Poly(styrene sulfonic acid) Transistors in Chemical and Biological Sensors. *Chem. Rec.* **2008**, *8*, 13–22.
- (2) Rivnay, J.; Owens, R. M.; Malliaras, G. G. The Rise of Organic Bioelectronics. *Chem. Mater.* **2014**, *26*, 679–685.
- (3) Luo, S. C.; Ali, E. M.; Tansil, N. C.; Yu, H. H.; Gao, S.; Kantchev, E. A. B.; Ying, J. Y. Poly(3,4-ethylenedioxythiophene) (PEDOT) Nanobiointerfaces: Thin, Ultrasooth, and Functionalized PEDOT Films with in Vitro and in Vivo Biocompatibility. *Langmuir* **2008**, *24*, 8071-8077.
- (4) Zhu, B.; Luo, S. C.; Zhao, H.; Lin, H. A.; Sekine, J.; Nakao, A.; Chen, C.; Yamashita, Y.; Yu, H. H. Large enhancement in neurite outgrowth on a cell membrane-mimicking conducting polymer. *Nat. Commun.* **2014**, *5*, 4523.
- (5) Yamato, H.; Ohwa, M.; Wernet, W. Stability of Polypyrrole and Poly(3,4-ethylenedioxythiophene) for Biosensor Application. *J. Electroanal. Chem.* **1995**, *397*, 163-170.
- (6) Balint, R.; Cassidy, N. J.; Cartmell, S. H. Conductive Polymers: Towards a Smart Biomaterial for Tissue Engineering. *Acta Biomater.* **2014**, *10*, 2341–2353.
- (7) Wong, J. Y.; Langer, R.; Ingber, D. E. Electrically Conducting Polymers can Non invasively Control the Shape and Growth of Mammalian Cells. *Proc. Natl. Acad. Sci. U. S. A.* **1994**, *91*, 3201–3204.

- (8) Saltó, C.; Saindon, E.; Bolin, M.; Kanciurzevska, A.; Fahlman, M.; Jager, E. W. H.; Tengvall, P.; Arenas, E.; Berggren, M. Control of Neural Stem Cell Adhesion and Density by an Electronic Polymer Surface Switch. *Langmuir* **2008**, *24*, 14133–14138.
- (9) Svennersten, K.; Bolin, M. H.; Jager, E. W. H.; Berggren, M.; Richter-Dahlfors, A. Electrochemical Modulation of Epithelia Formation Using Conducting Polymers. *Biomaterials* **2009**, *30*, 6257–6264.
- (10) Wan, A. M. D.; Brooks, D. J.; Gumus, A.; Fischbach, C.; Malliaras, G. G. Electrical Control of Cell Density Gradients on a Conducting Polymer Surface. *Chem. Commun.* **2009**, *35*, 5278–5280.
- (11) Wan, M. D.; Schur, R. M.; Ober, C. K.; Fischbach, C.; Gourdon, D.; Malliaras, G. G. Electrical Control of Protein Conformation. *Adv. Mater.* **2012**, *24*, 2501–2505.
- (12) Greco, F.; Fujie, T.; Ricotti, L.; Taccola, S.; Mazzolai, B.; Mattoli, V. Microwrinkled Conducting Polymer Interface for Anisotropic Multicellular Alignment. *ACS Appl. Mater. Interfaces* **2013**, *5*, 573–584.
- (13) Sivaraman, K. M.; Özkale, B.; Ergeneman, O.; Lühmann, T.; Fortunato, G.; Zeeshan, M. A.; Nelson, B. J.; Pané, S. Redox Cycling for Passive Modification of Polypyrrole Surface Properties: Effects on Cell Adhesion and Proliferation. *Adv. Healthcare Mater.* **2013**, *2*, 591–598.
- (14) Pires, F.; Ferreira, Q.; Rodrigues, C. A. V.; Morgado, J.; Ferreira, F. C. Neural Stem Cell Differentiation by Electrical Stimulation Using a Cross-Linked PEDOT Substrate: Expanding the Use of Biocompatible Conjugated Conductive Polymers for Neural Tissue Engineering. *Biochim. Biophys. Acta* **2015**, *1850*, 1158–1168.

- (15) Wan, A. M. D.; Chandler, E. M.; Madhavan, M.; Infanger, D. W.; Ober, C. K.; Gourdon, D.; Malliaras, G. G.; Fischbach, C. Fibronectin Conformation Regulates the Proangiogenic Capability of Tumor-Associated Adipogenic Stromal Cells. *Biochim. Biophys. Acta* **2013**, *1830*, 4314–4320.
- (16) Wan, M. D.; Inal, S.; Williams, T.; Wang, K.; Leleux, P.; Estevez, L.; Giannelis, E. P.; Fischbach, C.; Malliaras, G. G.; Gourdon, D. 3D Conducting Polymer Platforms for Electrical Control of Protein Conformation and Cellular Functions. *J. Mater. Chem. B. Mater. Biol. Med.* **2015**, *3*, 5040–5048.
- (17) Thomas, A.; Zong, K.; Schottland, P.; Reynolds, J. R. Poly(3,4-alkylenedioxyppyrole)s as Highly Stable Aqueous-Compatible Conducting Polymers with Biomedical Implications. *Adv. Mater.* **2000**, *12*, 222–225.
- (18) Proctor, M.; Rivnay, J.; Malliaras, G. G. Understanding Volumetric Capacitance in Conducting Polymers. *J. Polym. Sci. Part B: Polym. Phys.* **2016**.
- (19) Strakosas, X.; Wei, B.; Martin, D. C.; Owens R. M. Biofunctionalization of polydioxothiophene derivatives for biomedical applications. *J. Mater. Chem. B*, **2016**, *4*, 4952–4968
- (20) Karagkiozaki, V.; Karagiannidis, P. G.; Gioti, M.; Kavatzikidou, P.; Georgiou, D.; Georgarakis, E. Bioelectronics Meets Nanomedicine for Cardiovascular Implants: PEDOT-Based Nanocoatings for Tissue Regeneration. *Biochim. Biophys. Acta* **2013**, *1830*, 4294–4304.
- (21) Berggren, M.; Richter-Dahlfors, A. Organic Bioelectronics. *Adv. Mater.* **2007**, *19*, 3201–3213.

- (22) Collazos-Castro, J. E.; Polo, J. L.; Hernández-Labrado, G. R.; Padial-Cañete, V.; García-Rama, C. Bioelectrochemical Control of Neural Cell Development on Conducting Polymers. *Biomaterials* **2010**, *31*, 9244-9255.
- (23) Miriani, R. M.; Abidian, M. R.; Kipke, D. R. Cytotoxic Analysis of the Conducting Polymer PEDOT Using Myocytes. *30th Annual International IEEE EMBS Conference* **2008**, 20-24.
- (24) Teh, K. S.; Lu, Y. W. Surface Nanostructuring of Biocompatible Polymer for Wettability Control in MEMS. *21st Annual International IEEE MEMS Conference* **2008**, 363-366.
- (25) Marzocchi, M.; Gualandi, I.; Calienni, M.; Zironi, I.; Scavetta, E.; Castellani, G.; Fraboni, B. Physical and Electrochemical Properties of PEDOT:PSS as a Tool for Controlling Cell Growth. *ACS Appl. Mater. Interfaces* **2015**, *7*, 17993–18003.
- (26) Dalby, M. J.; Yarwood, S. J.; Johnstone, H. J.; Affrossman, S.; Riehle, M. O. Fibroblast Signaling Events in Response to Nanotopography: a Gene Array Study. *IEEE Trans. Nanobioscience* **2002**, *1*, 12-17.
- (27) Andersson, A. S.; Brink, J.; Lidberg, U.; Sutherland, D. S. Influence of Systematically Varied Nanoscale Topography on the Morphology of Epithelial Cells. *IEEE Trans. Nanobioscience* **2003**, *2*, 49-57.
- (28) Rice, J. M.; Hunt, J. A.; Gallagher, J. A.; Hanarp, P.; Sutherland, D. S.; Gold, J. Quantitative Assessment of the Response of Primary Derived Human Osteoblasts and Macrophages to a Range of Nanotopography Surfaces in a Single Culture Model in Vitro. *Biomaterials* **2003**, *24*, 4799-4818.

- (29) Dalby, M. J.; Riehlea, M. O.; Sutherlandb, D. S.; Aghelib, H.; Curtisa, A. S. G. Use of Nanotopography to Study Mechanotransduction in Fibroblasts: Methods and Perspectives. *Eur. J. Cell Biol.* **2004**, *83*, 159-169.
- (30) Vogel, V.; Sheetz, M. Local Force and Geometry Sensing Regulate Cell Functions. *Nat. Rev. Mol. Cell Biol.* **2006**, *7*, 265-275.
- (31) Brunetti, V.; Maiorano, G.; Rizzello, L.; Sorce, B.; Sabella, S.; Cingolani, R.; Pompa, P. P. Neurons Sense Nanoscale Roughness with Nanometer Sensitivity. *Proc. Natl. Acad. Sci. U.S.A.* **2010**, *107*, 6264–6269.
- (32) Lee, J. H.; Khang, G.; Lee, J. W.; Lee, H. B. Interaction of Different Types of Cells on Polymer Surfaces with Wettability Gradient. *J. Colloid Interface Sci.* **1998**, *205*, 323–330.
- (33) Ranella, A.; Barberoglou, M.; Bakogianni, S.; Fotakis, C.; Stratakis, E. Tuning Cell Adhesion by Controlling the Roughness and Wettability of 3D Micro/Nano Silicon Structures. *Acta Biomater.* **2010**, *6*, 2711–2720.
- (34) Sakmann, B.; Neher, E. *Single-Channel Recording*; Sakmann and Neher (Eds.): New York, 1995.
- (35) Levite, M.; Cahalon, L.; Peretz, A.; HersHKoviz, R.; Sobko, A.; Ariel, A.; Desai, R.; Attali, B.; Lider, O. Extracellular K⁺ and Opening of Voltage-Gated Potassium Channels Activate T Cell Integrin Function: Physical and Functional Association Between K_{v1.3} Channels and β 1 Integrins. *J.E.M.* **2000**, *191*, 1167-1176.

- (36) Lang, F.; Foller, M.; Lang, K. S.; Lang, P. A.; Ritter, M.; Gulbins, E.; Vereninov, A.; Huber, S. M. Ion Channels in Cell Proliferation and Apoptotic Cell Death. *J. Membrane Biol.* **2005**, *205*, 147–157.
- (37) Urrego, A. P.; Tomczak, F.; Zahed, W.; Stühmer, L.; Pardo, A. Potassium Channels in Cell Cycle and Cell Proliferation. *Philos. Trans. R. Soc. Lond. B. Biol. Sci.* **2014**, *369*, 20130094.
- (38) Higgins, M. J.; McGovern, S. T.; Wallace, G. G. Visualizing Dynamic Actuation of Ultrathin Polypyrrole Films. *Langmuir* **2009**, *25*, 3627–3633.
- (39) Zykwincka, A.; Domagala, W.; Pilawa, B.; Lapkowski, M. Electrochemical Overoxidation of Poly(3,4-ethylenedioxythiophene)—PEDOT Studied by Means of in Situ ESR Spectroelectrochemistry, *Electrochim. Acta* **2005**, *50*, 1625–1633.
- (40) Oostra, A. J.; Van Den Bos, K. H.; Blom, P. W.; Michels, J. J. Disruption of the Electrical Conductivity of Highly Conductive Poly(3,4-ethylenedioxythiophene):Poly(styrene sulfonate) by Hypochlorite. *J. Phys. Chem. B.* **2013**, *117*, 10929–10935.
- (41) Olsen, M. L.; Sontheimer, H. Mislocalization of K_{ir} Channels in Malignant Glia. *Glia* **2004**, *46*, 63–73.
- (42) Callies, C.; Fels, J.; Liashkovich, I.; Kliche, K.; Jeggle, P.; Kusche-Vihrog, K.; Oberleithner, H. Membrane Potential Depolarization Decreases the Stiffness of Vascular Endothelial Cells. *J. Cell Sci.* **2011**, *124*, 1936–1942.
- (43) Ransom, B.; Sontheimer, H. BK Channels in Human Glioma Cells. *J Neurophysiol.* **2001**, *85*, 790–803.

- (44) Guéguinou, M.; Chantôme, A.; Fromont, G.; Bougnoux, P.; Vandier, C.; Potier-Cartereau, M. K⁺Ca and Ca²⁺ Channels: the Complex Thought. *Biochim Biophys Acta*. **2014**, *1843*, 2322-2333.
- (45) Ridley, A. J.; Schwartz, M. A.; Burridge, K.; Firtel, R. A.; Ginsberg, M. H.; Borisy, G.; Parsons, J. T.; Horwitz, A. R. Cell Migration: Integrating Signals from Front to Back. *Science* **2003**, *302*, 1704-1709.
- (46) Ouadid-Ahidouch, H.; Roudbaraki, M.; Delcourt, P.; Ahidouch, A.; Joury, N.; Prevarskaya, N. Functional and Molecular Identification of Intermediate-Conductance Ca²⁺-Activated K⁺ Channels in Breast Cancer Cells: Association with Cell Cycle Progression. *Am. J. Physiol. Cell Physiol.* **2004**, *287*, C125-C134.
- (47) Blackiston, J.; McLaughlinand, K. A.; Levin, M. Bioelectric Controls of Cell Proliferation: Ion Channels, Membrane Voltage and the Cell Cycle. *Cell Cycle* **2009**, *8*, 3527-3536.
- (48) Berridge, M. J.; Bootman, M. D.; Lipp, P. Calcium - a Life and Death Signal. *Nature* **1998**, *395*, 645-648.